LASER INTERFEROMETER GRAVITATIONAL WAVE OBSERVATORY
- LIGO -
CALIFORNIA INSTITUTE OF TECHNOLOGY
MASSACHUSETTS INSTITUTE OF TECHNOLOGY

Technical Note **LIGO-T1800296–v1** 2018/08/03

Constructing a Homodyne Detector for Low Quantum Noise Gravitational Wave Interferometry

SURF Student: John Martyn
Mentors: Kevin Kuns, Aaron Markowitz, Andrew Wade, Rana Adhikari

California Institute of Technology
LIGO Project, MS 18-34
Pasadena, CA 91125
Phone (626) 395-2129
Fax (626) 304-9834
E-mail: info@ligo.caltech.edu

Massachusetts Institute of Technology
LIGO Project, Room NW22-295
Cambridge, MA 02139
Phone (617) 253-4824
Fax (617) 253-7014
E-mail: info@ligo.mit.edu

LIGO Hanford Observatory
Route 10, Mile Marker 2
Richland, WA 99352
Phone (509) 372-8106
Fax (509) 372-8137
E-mail: info@ligo.caltech.edu

LIGO Livingston Observatory
19100 LIGO Lane
Livingston, LA 70754
Phone (225) 686-3100
Fax (225) 686-7189
E-mail: info@ligo.caltech.edu

http://www.ligo.caltech.edu/

1 Introduction and Background

Achieving more efficient detection of gravitational radiation is a goal of contemporary experimental physics, as it will enable novel tests of general relativity and provide information on astronomical bodies that are difficult to observe through the electromagnetic spectrum. The gravitational waves (GWs) that encompass this radiation are described by oscillatory perturbations to a background spacetime metric. These waves manifest themselves physically by altering displacements in spacetime, such as spatial distances and time durations. Current GW observatories, such as LIGO, use high precision laser interferometry to detect miniscule changes in the length of interferometer arms, indicating the passage of a GW. Since typical changes in the LIGO arm lengths induced by GWs are of the order of 10^{-18} m, incredibly precise measurements must be conducted to observe a GW. In particular, LIGO uses a large Michelson interferometer furnished with Fabry-Perot cavities and power recycling mirrors to optimize its sensitivity and ability to detect GWs.

Despite their intricate designs, interferometric GW detectors are subject to various sources of noise that limit their resolution. Some of this noise arises from external sources, like human activity and weather patterns. The resulting noise can be combated by numerous techniques, such as performing interferometry in vacuum chambers and employing vibration isolation systems. Furthermore, on atomic and subatomic scales, new sources of intrinsic noise arise as the laws of quantum mechanics take precedence over those of classical physics. For instance, in quantum electrodynamics (QED), the quantized electromagnetic field reveals the discrete photon nature of light. This phenomenon introduces shot noise and radiation pressure noise into the interferometer due to the fact that the electromagnetic field of a beam of light is not smooth and continuous, but rather is composed of individual photons. Noise that arises from quantum mechanical processes is known as quantum noise and owes its existence to the Heisenberg uncertainty principle and quantum fluctuations. Because of these immutable laws, sources of quantum noise dictate that the sensitivity of classical GW interferometers is bounded below by the Standard Quantum Limit (SQL). For example, in a GW interferometer with arm lengths L, test masses of mass m, and detecting a GW of frequency Ω, the noise spectral density of the GW strain, h, is bounded below by [7]

$$S_h^{\mathrm{SQL}}(\Omega) = \frac{2\hbar}{m\Omega^2 L^2}. \tag{1}$$

In general, the SQL will differ depending on the precise interferometric setup, but the limitations it conveys remain the same.

However, it turns out that the SQL only applies to interferometers when the sources of noise are uncorrelated, as they are classically. In fact, despite its counterintuitive name, the SQL can be surpassed by cleverly constructed interferometers that take into account quantum mechanics and correlated noise. One such method of beating the SQL utilizes squeezed light and balanced homodyne detection. A balanced homodyne detector (BHD) is composed of two photodiodes, a 50/50 beam splitter, and two sources of light: the signal and the local oscillator. An image of a BHD setup is displayed in Figure 1. The signal is the light that contains the desired information; for instance, it could be the light coming from the main interferometer that encodes the structure of a passing GW. On the other hand, the local oscillator is a stabilized source of light with its carrier frequency equal to that of

the signal. In an interferometer, the local oscillator light can be obtained from the incident laser light before it reaches the main interferometer. In balanced homodyne detection, these two sources of light are first mixed by being sent through the beam splitter. Next, the two photodiodes measure the photocurrents induced by the two outgoing beams from the beam splitter. One can then measure and analyze these photocurrents, from which information about the quadratures can be extracted.

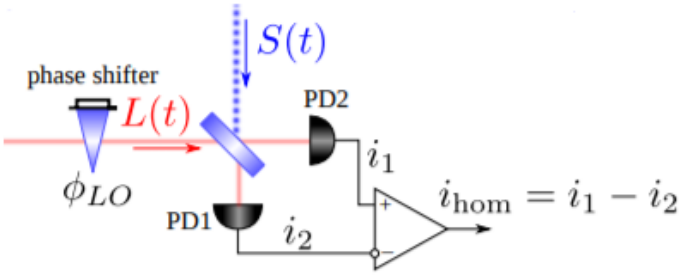

Figure 1: A standard BHD setup, obtained from [15].

Following the analysis presented in [15], we can describe this procedure mathematically. Let the electric fields of the signal and local oscillator light have quadratures $S_{c,s}(t)$ and $L_{c,s}(t)$, respectively, and carrier frequency ω:

$$S(t) = S_c(t)\cos(\omega t) + S_s(t)\sin(\omega t), \qquad L(t) = L_c(t)\cos(\omega t) + L_s(t)\sin(\omega t). \tag{2}$$

Due to inevitable quantum noise, the quadratures will contain terms due to noise. Denoting these by $n_{c,s}(t)$ and $l_{c,s}(t)$, respectively, the quadratures can be decomposed as

$$\begin{aligned} S_{c,s}(t) &= \text{signal} + \text{quantum noise} = G_{c,s}(t) + n_{c,s}(t) \\ L_{c,s}(t) &= \text{classical field} + \text{laser noise} = L^{(0)}_{c,s}(t) + l_{c,s}(t). \end{aligned} \tag{3}$$

Since the local oscillator is under the experimentalist's control, we will impose on it a phase shift, ϕ_{LO}, known as the homodyne angle: $L^{(0)}_c(t) = L_0\cos(\phi_{LO})$, $L^{(0)}_s(t) = L_0\sin(\phi_{LO})$. Such an alteration could be realized by changing the path length of the local oscillator. Additionally, we will assume that the local oscillator's amplitude is much greater than the other amplitudes in this scenario: $L_0 \gg G_{c,s}, n_{c,s}, l_{c,s}$. Under these assumptions, one can calculate the ideal photocurrents induced at the two photodiodes, which we denote by i_1 and i_2. In balanced homodyne readout, one chooses not to measure these currents, but instead measures the difference between them: $i_{\text{hom}} = i_1 - i_2$. To first order in $G_{c,s}, n_{c,s}$, and $l_{c,s}$, this is given by [15]

$$i_{\text{hom}} \propto L_0((G_c + n_c)\cos(\phi_{LO}) + (G_s + n_s)\sin(\phi_{LO})). \tag{4}$$

Evidently, this expression is independent of $l_{c,s}$, so the noise from the local oscillator does not factor into measurements of i_{hom}. In addition, Eq. (4) indicates that, by varying ϕ_{LO} and measuring i_{hom}, one can measure the signal's quadratures and linear combinations of them, with a precision limited only by the quantum noise of the signal.

In an interferometric GW detector, acquisition of the quadratures provides accurate information about the passing gravitational radiation. Thus, a properly constructed BHD presents the opportunity to probe exceptionally small length scales and improve GW detection. However, the real world is not so ideal. In the construction of a physical BHD, other sources of optical and electronic noise exist within the interferometer. The optical noise arises from noise present in the signal, and the electronic noise emerges from noise induced in the detector. For instance, an imperfect beam splitter will create an imbalance in the light beams emerging from it and introduce local oscillator noise into i_{hom}. In addition, this setup is susceptible to noise in its electronic circuits, such as thermal noise in the resistors and intrinsic $1/f$ noise. In order to analyze the noises within the electronic circuits, one must calculate the noise spectral density of each circuit element. Let the noise spectral density of the j^{th} circuit element be denoted by e_{n0j}. The exact form of e_{n0j} will differ for distinct circuit elements since their noise contributions will not be the same. Then, the noise voltage due to this element, denoted by E_{n0j}, is obtained via

$$E_{n0j}^2 = \int_0^\infty df \ |e_{n0j}|^2. \tag{5}$$

Generally, this integral will be limited by the finite bandwidth over which the circuit operates. Finally, the total noise voltage due to all the circuit elements, denoted by E_{n0}, can be obtained from an RMS summation:

$$E_{n0}^2 = \sum_j E_{n0j}^2. \tag{6}$$

Proper analyses of all of these noises must be incorporated in order to correctly interpret the data from a BHD.

Current gravitational wave observatories do not exploit balanced homodyne detection of this sort. Instead, these experiments primarily use DC readout [14], in which a single photodetector measures the light output from the main interferometer's beam splitter. As shown in [15], DC readout schemes are affected by the noise in the local oscillator, unlike ideal balanced homodyne readout. In addition, DC readout schemes are not as effective as balanced homodyne readout at measuring arbitrary quadratures of light in an interferometer. This is best done by using squeezed light and a BHD with a variable homodyne angle, which enables one to take advantage of the reduced quadrature uncertainties of the squeezed light. Therefore, it is believed that balanced homodyne detection will provide more precise interferometric measurements in GW detectors than the current DC readout schemes do. We hope that further research into this technology will lead to the implementation of balanced homodyne detectors in GW interferometers and improved detection of gravitational radiation.

2 Approach

The goal of this project will be to construct a balanced homodyne detector. Once completed, we will then analyze the electronic and optical noise that exists within the BHD. The BHD will be constructed from standard optical devices used in interferometry, including a laser,

beam splitters, and photodiode detectors. More specifically, we will use InGaAs photodiodes. These are optimal for this setup because they have a high quantum efficiency and convert incident light into photocurrent very effectively. To amplify the interferometric signal and convert it from a current signal to a voltage signal, we will implement transimpedance amplifiers with low current noise. The specific transimpedance amplifiers to be used are homemade ones from the Adhikari lab, and it is desired that they contribute a minimal level of electronic noise. An image of a sample transimpedance amplifier circuit, which will be used as a guide in the BHD construction, is displayed in Figure 2.

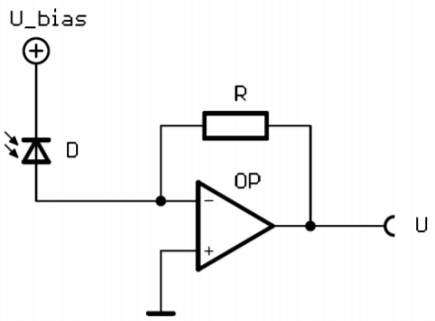

Figure 2: A basic transimpedance amplifier circuit, obtained from [5]. This circuit contains a photodiode (D), a resistor (R), and an operational amplifier (OP). U_bias and U denote the bias and output voltages, respectively.

Moreover, in order to analyze the optical and electronic noise in these devices, we will utilize two programs known as LISO and Finesse. LISO will be used to optimize electronic noise, and Finesse will be used to simulate the noise in the interferometer. Proper application of both programs is central to gauging the success of the final homodyne detector. Lastly, when a mathematical analysis of the noise in the BHD is required, Python Jupyter notebooks will be used to carry out analytic calculations and plot results.

3 Progress

3.1 Week 1

During my first week at Caltech, I began my project by studying additional material on gravitational wave interferometry, signal modulation, random processes, and noise. In particular, I read through sections of [15] and [11], which covered each of these topics. Learning more about these subjects has helped me better understand gravitational wave interferometry and the methods used to combat the noise in GW detectors. In addition, I familiarized myself with LTspice, a computer program used to model and simulate electronic circuits. LTspice can be employed to study the functionality of a circuit design and investigate the noise that exists within it. The ability to perform these operations easily via computer software will be of utmost importance to me when I analyze the electronic noise in the BHD. Lastly, I was

taught about laboratory safety procedures, such as those pertaining to laser usage, so that I may work in the lab without causing harm.

3.2 Week 2

At the beginning of the next week, I started to work with photodiode amplifiers. These devices will be incorporated into the BHD in order to strengthen any optical signal detected. In addition to studying the noise produced by photodiode amplifiers in [9], I constructed sample photodiode amplifier circuits, and conducted measurements on them to ensure that they function properly. The amplifiers I built are akin to that in Figure 2; in my amplifiers, I incorporated an MTD5052W photodiode, an LT1028 op-amp, and 7.5 kΩ and 1 kΩ resistors. One of these amplifiers is intended to be used in the photodiode in the LIGO outreach miniature interferometer. In the coming weeks, I plan solder this amplifier onto a circuit board and encase it in a 3D printed container so that it can be easily incorporated into the outreach interferometer.

Furthermore, I began constructing the BHD during this time. This consisted of setting up a 1064 nm Nd:YAG laser, wave plates, a Faraday rotator, a beam splitter, and beam dumps. A picture of the current setup is displayed below in Figure 3. The wave plates and Faraday rotator are used to alter the polarization of the light emitted by the laser. Our setup of these elements forms an optical isolator, in which light is transmitted only in the forward direction. This ensures that no back-scattered light interferes with the laser light. By tweaking the relative phase shift imparted onto the light by the wave plates and the Faraday rotator, this setup allows us to block certain polarizations of light and control the amount of light that will enter the BHD. In effect, this gives us control over the strength of the light in the BHD interferometer. Next, the beam splitter splits the light that exits the Faraday rotator and will be an integral component of the interferometer. Lastly, the beam dumps capture scattered and reflected light produced by this setup, which would otherwise interfere with the light in the BHD and pose a threat to our safety.

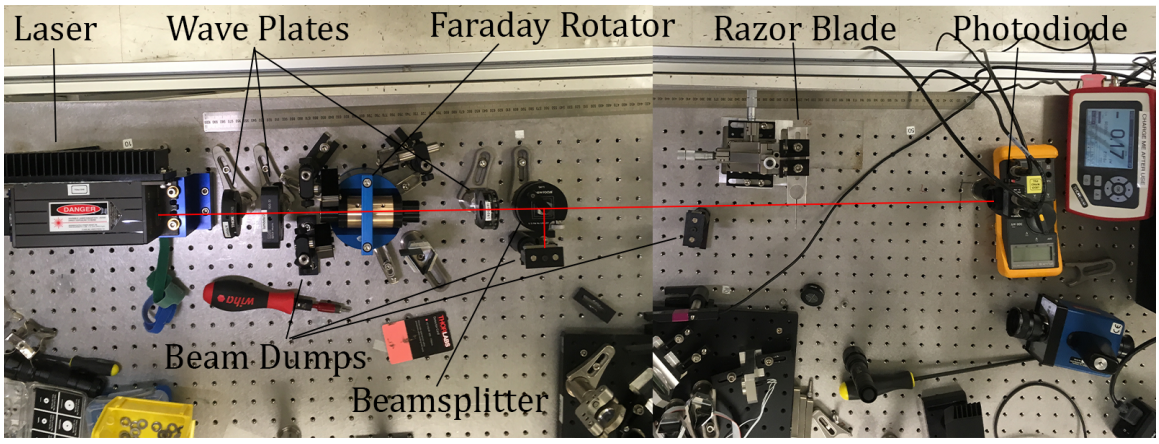

Figure 3: Our current BHD setup, including a laser, wave plates, a Faraday rotator, a beam splitter, and beam dumps. The razor blade and photodiode will be discussed in the next section.

3.3 Week 3

During my third week, I learned how to solder electronic circuits by constructing a simple RC lowpass filter that will be used in the LIGO outreach interferometer. This simple circuit consisted of a 430 Ω resistor in series with a 1.5 μF capacitor; a schematic of the circuit is pictured below in Figure 4. This circuit has a cutoff frequency of 250 Hz, and is designed to pass low frequency signals to an audio amplifier.

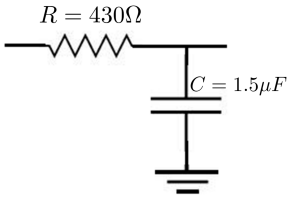

Figure 4: A schematic of the RC lowpass filter.

Moreover, I also studied Gaussian beams, which describe the electromagnetic waves emitted by lasers. In particular, I read Kogelnik and Li's article on Gaussian beams [6], which covered numerous concepts about the light produced by lasers and resonators. Mathematically, a Gaussian beam is a paraxial beam of light that can be expanded into transverse electromagnetic modes, characterized by $m, n \in \mathbb{N}_0$ and denoted by TEM_{mn}. The simplest mode, is the TEM_{00} mode. If the beam propagates along the z direction with a wave number, k, the x and y components of the electric field of the TEM_{00} mode are [2]:

$$E_{x,y}(\vec{x},t) = E_{x,y0}\left(\frac{w_0}{w(z)}\right)e^{\frac{-r^2}{w(z)^2}}e^{i(kz-\omega t+\frac{kr^2}{2R(z)}+\alpha(z))}, \quad r^2 = x^2+y^2. \tag{7}$$

Here, $w(z)$ is the beam waist, which takes a minimum value of w_0:

$$w(z) = w_0\sqrt{1+(z/z_R)^2}; \tag{8}$$

z_R is the Rayleigh range:

$$z_R = \frac{1}{2}kw_0^2; \tag{9}$$

$R(z)$ is the beam's radius of curvature:

$$R(z) = z + z_R^2/z; \tag{10}$$

and $\alpha(z)$ is the Gouy phase:

$$\alpha(z) = -\arctan(z/z_R). \tag{11}$$

For our BHD setup, we desire the light entering the interferometer to be a stable TEM_{00} mode. In order to determine the identity of the light being emitted by the laser, I conducted beam profiling on our setup. Specifically, I first chose five locations along the lab bench, each equally spaced by 10 cm and located at different distances from the laser. At each point I placed a horizontal razor blade in front of the beam. I then varied the height of the razor blade so that it blocked part of the beam, and simultaneously measured the voltage produced

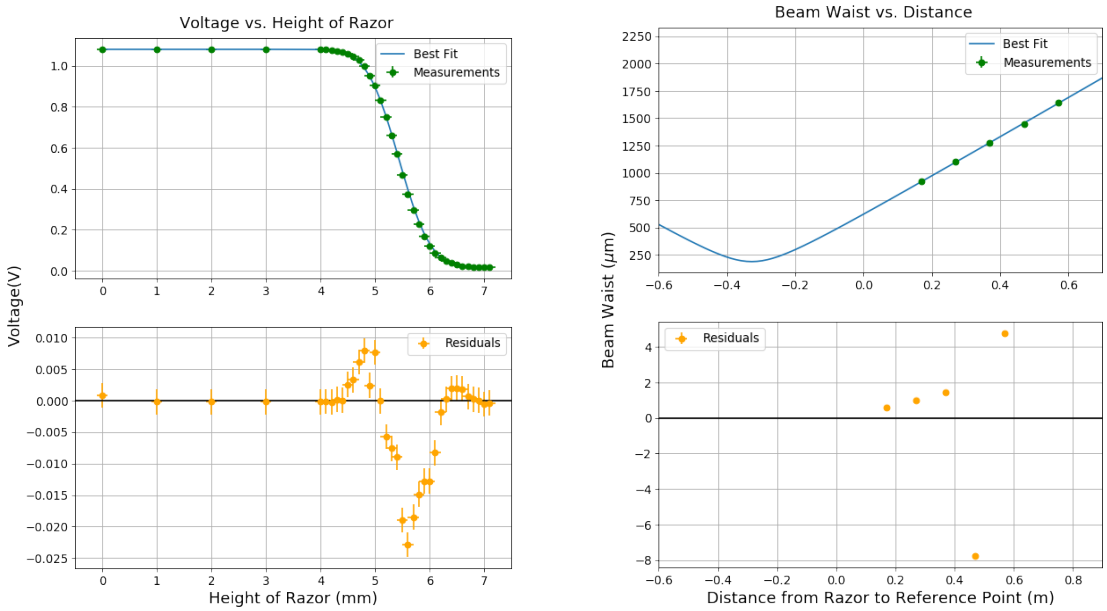

Figure 5: Left: Voltage measurements and line of best fit at the first measurement location. Right: Beam waist measurements and line of best fit.

by a photodiode in the path of the beam. The placements of the razor and photodiode are shown in Figure 3.

The photodiode responds to the beam by generating a voltage in response to the power it receives from the beam. With the razor blade at height u from the center of the beam, the power received by the photodiode is (ignoring diffraction effects)

$$P(z) = \int I(\vec{x})dA \propto \int_{-\infty}^{\infty}\int_{u}^{\infty} dxdy\Big(\frac{w_0}{w(z)}\Big)^2 e^{-\frac{2r^2}{w(z)^2}} \propto w_0^2\Big(1-\text{erf}\Big(\frac{\sqrt{2}u}{w(z)}\Big)\Big). \tag{12}$$

Next, we expect the voltage produced by the photodiode to be linear in the power it receives. However, I must note that the height of the razor blade that I recorded, denoted by h, is not equal to the height above the center of the beam, which is u. Instead, there is a constant difference between these: $u = h + b$, where b is parameter corresponding to the height of $h = 0$ above the center of the beam. Taking this into account, we expect

$$V(h,z) = V_0 + a\Big(1-\text{erf}\Big(\frac{\sqrt{2}(h+b)}{w(z)}\Big)\Big), \tag{13}$$

where V_0, a, b, and $w(z)$ are variable parameters at each location. I then fit the data to this curve in a Jupyter notebook by minimizing $\chi^2 = \sum_i \left(\frac{V_i - V(h_i,z)}{\sigma_i}\right)^2$ with respect to the parameters. The voltage data and the curve of best fit obtained at the first location are displayed above in Figure 5. The fits at the other four locations were quite similar. In general, the fits appear pretty good and the residuals are low in magnitude. However, the residuals display a distinct pattern and are not randomly distributed. Therefore, it is likely that there is an effect not accounted for in this fit, such as diffraction or a non-TEM_{00} mode contaminating the laser beam.

Once these fits were completed, I had obtained five empirical values of $w(z)$ at different distances from the laser. Specifically, I recorded the distances from the razor blade to a reference point near the laser, which I chose to be the base of a beam dump, and denoted this quantity by D. This distance differs from z in our coordinate system by a constant: $z = D + c$. With this fact noted, I then fit these empirical values to $w(z)$ specified in Eq. (8) by treating w_0 and c as fitting parameters and minimizing χ^2. Doing so yielded a minimum beam waist of $w_0 = 1.871 \cdot 10^{-4} \pm 1.419 \cdot 10^{-9}$ m and a constant offset of $c = 0.3274 \pm 4.557 \cdot 10^{-6}$ m, both of which are reasonable values for this laser and setup. The data and fit for the beam waist are displayed above in Figure 5.

3.4 Week 4

During my fourth week, I began working with LISO, a program that can be used to simulate circuits and analyze their properties, including their transfer functions and noise. Since LISO is run through the Linux terminal, I access it by logging onto the cymac computer in QuIL. Most of my LISO calculations have been performed through a Jupyter notebook with pyliso, a Python wrapper for LISO written by Craig, Andrew, Kevin, and Anchal that facilitates its use.

After installing LISO and running some tests in it, I started using it to design the transimpedance amplifier circuits that will be incorporated into in our BHD. For these circuits, we desire the electronic noise to be at least 10 dB less than the shot noise of the light over a bandwidth of at least 10 kHz. In terms of the noise spectral density, $s(f) = \sqrt{S(f)}$, this requires

$$s_{\text{electronic}}(f) < \frac{1}{\sqrt{10}} s_{\text{shot}}(f). \tag{14}$$

At this time, I planned to use the circuit in Figure 6 in order to accomplish this goal. In this schematic, the photodiode is represented by the diode D1 in parallel with a capacitor $C3$, representing the capacitance of the photodiode. To the right of the photodiode is the transimpedance amplifier, containing a feedback resistor R_F, a feedback capacitor C_F, and a series resistor $R3$. To the left of the photodiode is a lowpass filter with Sallen-Key topology. This was included to filter out noise arising from signals outside of our bandwidth of interest. This Sallen-Key filter has a $1/f^2$ roll off past the cutoff frequency $f_c = \frac{1}{2\pi\sqrt{R_1 R_2 C_1 C_2}}$, and thus attenuates unwanted frequencies better than an ordinary passive RC filter. Lastly, I decided to use OP27 op amps in both the amplifier and filter as the OP27 has a low noise of $3.5 \frac{\text{nV}}{\sqrt{\text{Hz}}}$ and a large gain bandwidth product of 8 MHz, so it should perform well without drastically increasing electronic noise. Once this design was chosen, I then sought to employ LISO to optimize the resistance and capacitance values in the circuit in order to achieve our desired low level of noise.

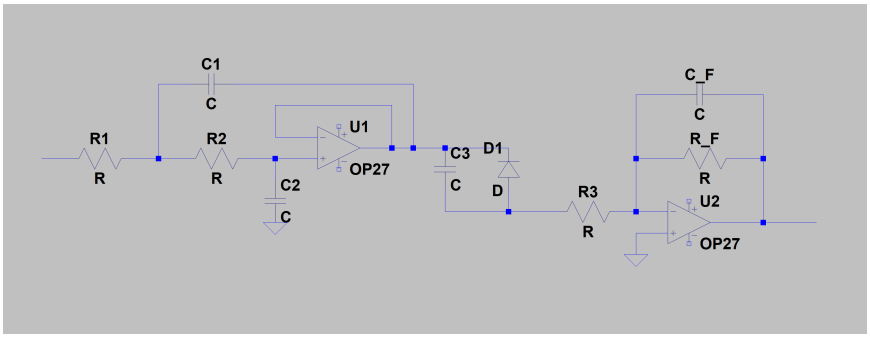

Figure 6: A schematic of the planned photodiode circuit.

3.5 Week 5

From Monday to Wednesday of this week, I traveled to Louisiana with the rest of the LIGO SURF group to visit LIGO Livingston. There, we learned a good deal about the LIGO detectors had a great time touring New Orleans.

Upon returning to Caltech, I continued my work with the photodiode circuits to be used in the BHD. I referenced [19] and [20] to determine the ideal resistance and capacitance values for the amplifier, using LIGO's amplifier design as a template. Similarly, the resistance and capacitance values of the Sallen-Key filter were chosen to block DC signals, cutting off frequencies less than 0.1 Hz. Lastly, I constructed the circuit and placed 100 nF bypass capacitors at the + and − terminals of the amplifier's om amp in order to provide a clean input voltage and reduce noise.

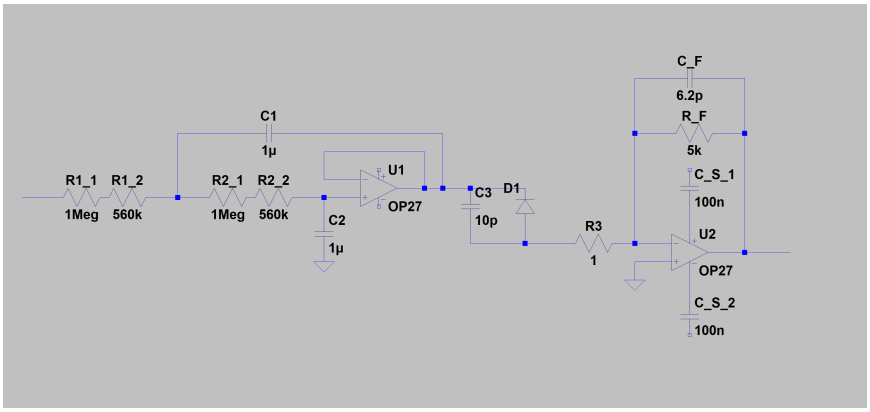

Figure 7: A schematic of the improved photodiode circuit.

As mentioned previously, we aimed to have the amplifier's electronic noise be 10 dB less than the shot noise. Our photodiodes will be subjected to a 1064 nm laser operating at a power of $P = 1$ mW. Assuming the photodiodes have a perfect quantum efficiency of $\eta = 1$, the shot noise spectral density should be

$$s_{\text{shot}}(f) = R_F\sqrt{2eI} = R_F\sqrt{2e\frac{\eta eP}{h\nu}} = 8.95 \cdot 10^{-8}\ \frac{\text{V}}{\sqrt{\text{Hz}}}. \tag{15}$$

By Eq. 14, we require

$$s_{\text{electronic}} < \frac{1}{\sqrt{10}} 8.95 \cdot 10^{-8} \frac{\text{V}}{\sqrt{\text{Hz}}} = 2.83 \cdot 10^{-8} \frac{\text{V}}{\sqrt{\text{Hz}}} =: s_{max}(f) \tag{16}$$

for the amplifier circuit. To determine if this limit had been reached, I simulated the amplifier in LISO and calculated its noise. The resulting plot, shown in Figure 8, indicates that the amplifier reaches a noise floor of 10 $\frac{\text{nV}}{\sqrt{\text{Hz}}}$, satisfying the aforementioned bound.

In theory then, this circuit ought to obtain our desired level of noise. To determine if this is the case in practice, I constructed the amplifier and measured its noise with the SR785 spectrum analyzer in the electronics shop. The results are shown against the LISO predictions in Figure 8. The measured noise floor is roughly $11 \frac{\text{nV}}{\sqrt{\text{Hz}}}$ over a bandwidth greater than 10 kHz, which satisfies our noise requirement. However, the measured noise floor is slightly greater than the theoretical value, which I believe to be due to the noise limitations of the spectrum analyzer. With no input signal, the SR785 measures a noise floor of roughly $s_{\text{SR785}} = 5 \frac{\text{nV}}{\sqrt{\text{Hz}}}$. This additional noise ought to be incorporated into the measured electronic noise by RMS summation:

$$s_{\text{electronic,measured}} = \sqrt{s^2_{\text{electronic,theoretical}} + s^2_{\text{SR785}}} = \sqrt{10^2 + 5^2} \frac{\text{nV}}{\sqrt{\text{Hz}}} = 11.18 \frac{\text{nV}}{\sqrt{\text{Hz}}}. \tag{17}$$

This agrees well with our measured noise floor, indicating that the additional noise was likely caused by the limited capabilities of the SR785. Furthermore, the large spikes in the measured noise spectral density can be attributed to external noise sources, such as 60 Hz noise (and its harmonics) and RF signals from devices in nearby labs interfering with my measurements.

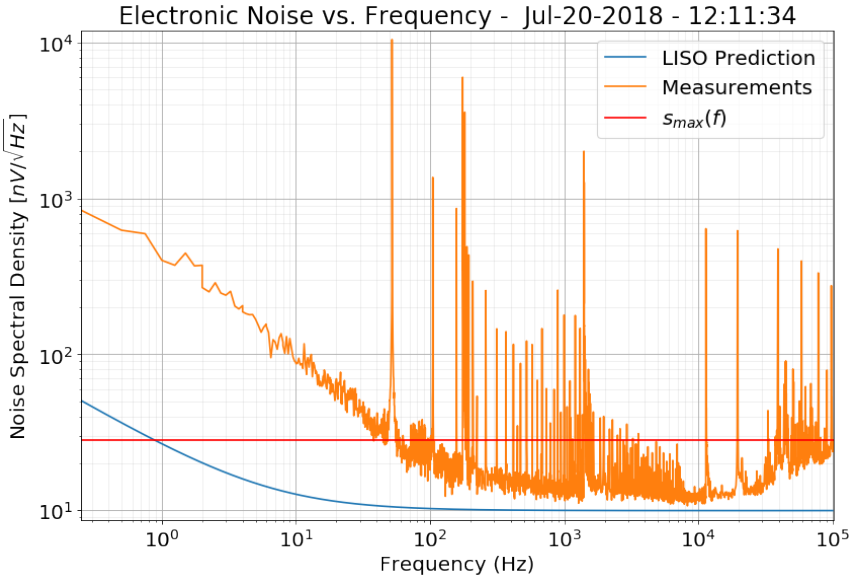

Figure 8: Plots of theoretical noise and measured noise.

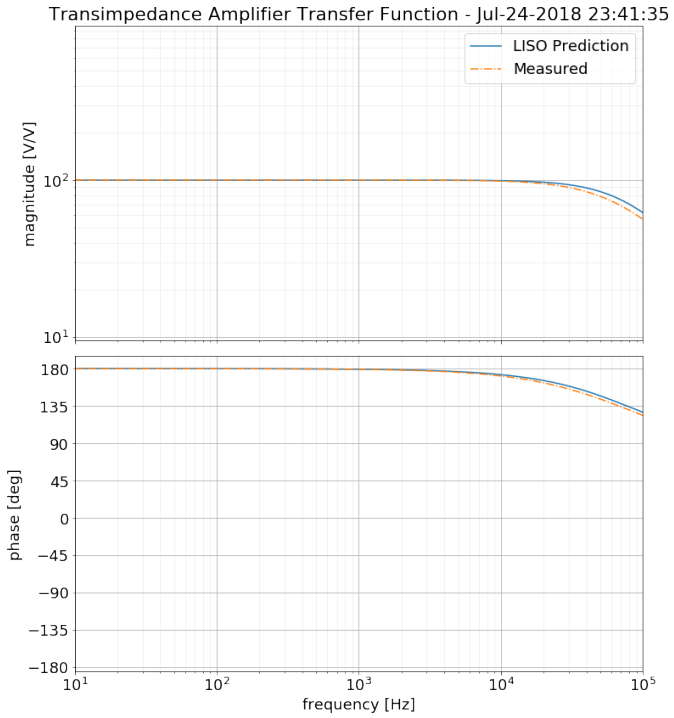

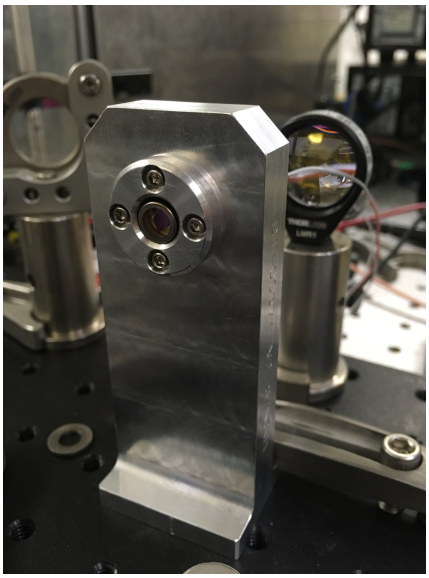

Figure 9: Left: Plots of theoretical and measured transfer functions of the transimpedance amplifier. Right: A picture of our Laser Components InGaAs PIN photodiode.

3.6 Week 6

My next goal was to measure the transfer function of the transimpedance amplifier. I was able to perform this measurement with the SR785 in the 40m lab over the frequency range of 10 Hz - 100 kHz. The resulting data is plotted below against the LISO predictions in Figure 9. Evidently, the measured transfer function agrees well with the predicted one, both displaying a gain of roughly 100. However, the measured transfer function appears to roll off slightly before the predicted transfer function; I suspect that this discrepancy could possibly be caused by parasitic capacitance or inductance in the breadboard that was not incorporated into LISO.

Thus far, the transimpedance amplifier behaved as expected. I then aimed to study the combined behavior of the photodiodes and the amplifier. The photodiodes we will use are Laser Components InGaAs PIN photodiodes; their model number is IG17X3000G1i. A picture of one of these photodiodes is shown in Figure 9.

In order to characterize the response of these photodiodes to a signal, we needed to measure the current-voltage transfer function of the photodiode and transimpedance amplifier circuit. Kevin and I carried out this measurement with the Jenne laser and Agilent in the 40m lab. Our first attempt to perform this measurement failed, likely due to a broken op amp or a misaligned laser. After constructing a new, identical circuit, we successfully measured the current-voltage transfer function, and Figure 10 depicts our measurements over the modulation frequency range of 30 kHz-30 MHz when the power of the laser was set to 69 μW and 95 μW. These plots indicate that our setup behaves stably over the frequency

range of interest, and has a clear roll off frequency around 300 kHz. As such, we believe that this setup is well-behaved and ready for implementation in the BHD.

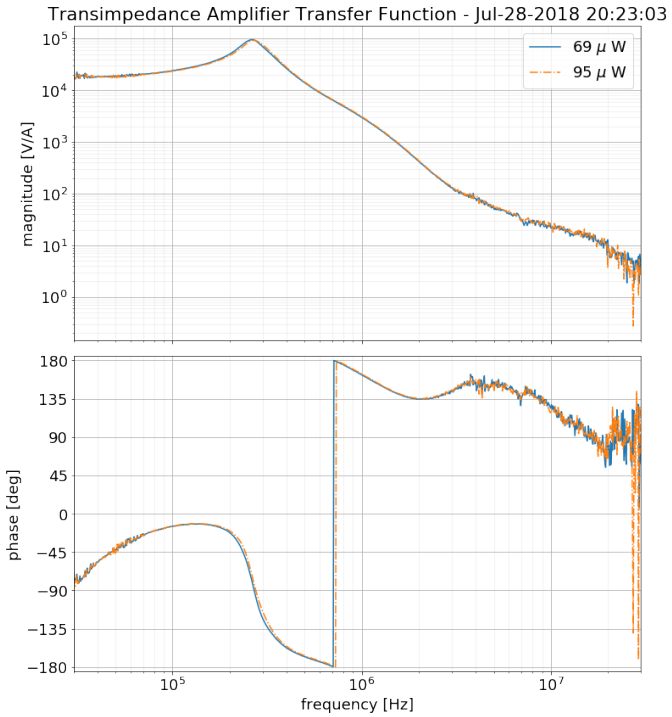

Figure 10: Plots of the current-voltage transfer function of the photodiode and amplifier setup.

3.7 Week 7 and Future Work

The next step in this project is to further optimize the photodiode transimpedance amplifier circuit, and incorporate them into a signal subtraction scheme for the BHD. In doing so, we have opted to remove the Sallen-Key filter in favor of adding a passive RC filter, a buffer, and a differential amplifier. These components will filter and stabilize the output signal and make it easier to send the signal to an analog to digital converter for subtraction. I was also advised to remove the resistor in series with the photodiode to increase the gain of the amplifier. A schematic of the new circuit is shown in Figure 11.

Currently, I have constructed two of these circuits and hooked them up to our BHD setup in QuIL. A picture of one of these circuits is shown in Figure 11. Our plan is to measure the noise in this setup to ensure that it will allow us to attain our desired signal to noise ratio. To perform this measurement, we will send in a signal modulated by the laser or an acousto-optical modulator, and measure the output signal and noise with the SR785. Once this task and the subtraction mechanism are completed, we will aim to construct the rest of the BHD, such as the local oscillator and additional optical components.

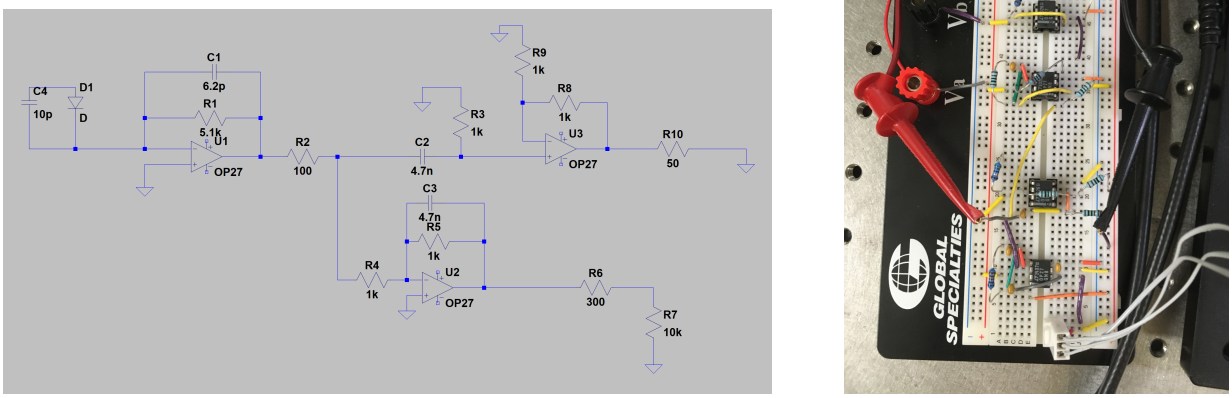

Figure 11: Left: Schematic of the new circuit connected to the photodiode. Right: The modified transimpedance amplifier circuit.

References

[1] A. I. Lvovsky, *Squeezed Light*. ArXiv e-prints (2016), arXiv:1401.4118v2 [quant-ph].

[2] A. Zangwill, *Modern Electrodynamics*. (2013)

[3] B.P. Abbott et al., *Observation of Gravitational Waves from a Binary Black Hole Merger*. Phys. Rev. Lett. **116**, 061102 (2016).

[4] C. W. Misner, K. S. Thorne, and J. A. Wheeler, *Gravitation*. (1973).

[5] H. Grote, et. al., *High power and ultra-low-noise photodetector for squeezed-light enhanced gravitational wave detectors*. Opt. Express, **24**, 20107-20118 (2016).

[6] H. Kogelnik and T. Li, *Laser Beams and Resonators*. Appl. Opt. **5**, 1550-1567 (1966)

[7] H. Miao, *Exploring Macroscopic Quantum Mechanics in Optomechanical Devices*. (2012).

[8] H. W. Ott, *Noise Reduction Techniques in Electronic Systems*. (1988).

[9] J. G. Graeme, *Photodiode Amplifiers: Op Amp Solutions*. (1995).

[10] K. Thorne, *Ph237b: Gravitational Waves*. California Institute of Technology (2002).

[11] K. Thorne and R. Blanford *Modern Classical Physics: Optics, Fluids, Plasmas, Elasticity, Relativity, and Statistical Physics*. (2017).

[12] https://www.ligo.caltech.edu/

[13] M. Bassan, et. al, *Advanced Interferometers and the Search for Gravitational Waves*. (2014).

[14] K. Nakamura and M. Fujimoto *Double balanced homodyne detection*. ArXiv e-prints (2018), arXiv:1711.03713v2 [quant-ph].

[15] S. L. Danilishin and F. Y. Khalili, *Quantum Measurement Theory in Gravitational-Wave Detectors*. ArXiv e-prints (2012), arXiv:1203.1706v2 [quant-ph].

[16] S. M. Carroll, *Spacetime and Geometry: An Introduction to General Relativity*. (2004).

[17] W. Ketterle, *8.422 Atomic and Optical Physics II*. Spring 2013. Massachusetts Institute of Technology: MIT OpenCourseWare, https://ocw.mit.edu. License: Creative Commons BY-NC-SA.

[18] G. Heinzel, NAO Mitaka, *LISO - Program for Linear Simulation and Optimization of analog electronic circuits Version 1.7*. (1999), http://www2.mpq.mpg.de/~ros/geo600_docu/soft/liso/manual.pdf.

[19] H. Hashemi, *Transimpedance Amplifiers (TIA): Choosing the Best Amplifier for the Job*. (2012), http://www.tij.co.jp/jp/lit/an/snoa942a/snoa942a.pdf.

[20] A. Bhat, *Stabilize Your Transimpedance Amplifier*. (2012), https://www.maximintegrated.com/en/app-notes/index.mvp/id/5129.